Rhodopsin Activity Varies in Proteoliposomes Prepared by Different Techniques

Shui-Lin Niu, Brian Doctrow, and Drake C. Mitchell*

Laboratory of Membrane Biochemistry and Biophysics, National Institute on Alcohol Abuse and Alcoholism, National Institutes of Health, Bethesda, Maryland 20892-9410

ABSTRACT: A variety of techniques are currently in use for preparing protein-containing lipid vesicles known as proteoliposomes. However, the functionality of membrane protein in proteoliposomes prepared by various techniques has rarely been evaluated directly. We prepared rhodopsin-containing proteoliposomes consisting of asolectin or native retinal rod outer segment disk lipids using *n*-octyl β-D-glucopyranoside and the detergent dialysis (DD) and rapid dilution (RD) techniques and measured the activity of rhodopsin using equilibrium UV/vis and flash photolysis spectroscopy. A significant difference in rhodopsin activity was observed in proteoliposomes prepared by these techniques. The equilibrium constant of metarhodopsin I–metarhodopsin II is 30–45% higher, and the apparent rate constant of MII formation is up to 3-fold faster in proteoliposomes prepared by RD vs DD. The DD technique produced larger yet more heterogeneous vesicles, while the RD technique yielded smaller and more homogeneous vesicles, as determined by electron microscopy and isopicnic centrifugation. Both proteoliposomes and empty lipid vesicles lacking rhodopsin were formed in the DD preparation, while only proteoliposomes were formed in the RD preparation. Under identical conditions, proteoliposomes prepared by RD have a higher L/P ratio, which is consistent with the higher level of rhodopsin activity in RD proteoliposomes. Overall, the results presented here suggest that the RD technique has an advantage over the DD technique in terms of preserving optimal rhodopsin activity and controlling the lipid to protein ratio in the final proteoliposomes.

Membrane proteins make up about 25% of the mammalian genome (*1*, *2*) and are essential to a variety of important biological processes. Typical biological membranes consist of a large number of different lipid species and multiple integral and membrane-bound proteins. This organizational and constituent complexity of biological membranes makes it difficult to obtain detailed structural and functional information on individual membrane proteins in situ. This complexity also makes it difficult to characterize molecular interactions between various lipids and proteins, which are vital to the understanding of membrane functions. A common approach to reduce the complexity of biological membranes is to isolate the membrane protein of interest and reconstitute it into lipid vesicles known as proteoliposomes. When properly constructed, the lipid composition and lipid-to-protein ratio (L/P ratio)[1] can be precisely controlled. This technique has been applied to many classes of membrane proteins including membrane transporters (*3*), membrane receptors (*4*), ion channels (*5*), and many other systems (*6–12*) and has contributed significantly toward our current under-

standing on the structure and function of membrane proteins (*13–15*).

Several techniques have been developed to prepare proteoliposomes, including the use of mechanical force, freeze–thaw cycles, organic solvents, or detergents (*4, 13, 16, 17*). The most widely adopted techniques, however, are detergent-based preparation, since the structure and function of membrane proteins are restored and maintained with the proper selection of detergents (*13–15*). The detergent-based preparation of proteoliposomes involves cosolublization of membrane proteins and lipids in detergent micelles followed by a detergent removal step to induce the formation of proteoliposomes. The two most commonly used procedures for detergent removal are detergent dialysis (DD) and rapid dilution (RD). The DD technique involves a gradual removal of detergents under an equilibrium condition, while the RD technique uses an instantaneous dilution step to lower the detergent concentration below its critical micellar concentration (cmc) followed by a dialysis step to remove the remaining detergent monomers.

Currently, the preparation of proteoliposomes remains empirical and is a matter of preference among different groups. It is often difficult to compare results derived from different studies, since little is known about the impact of different preparations of proteoliposomes on the structure and function of membrane proteins. This study was undertaken to explore the potential relationship between the method of proteoliposome preparation and the structure and function of a membrane protein.

Rhodopsin is the prototypical member of the superfamily of G protein-coupled receptor (GPCR), and its high-resolu-

* To whom correspondence should be addressed at the Department of Physics, Portland State University, P.O. Box 751, Portland, OR 97207-0751. Phone: 503-725-9876. Fax: 503-725-2815. E-mail: drakem@pdx.edu.

[1] Abbreviations: cmc, critical micelle concentration; DD, detergent dialysis; RD, rapid dilution; L/P ratio, lipid-to-protein ratio; MI, metarhodopsin I; MII, metarhodopsin II; K_{eq}, equilibrium constant for the MI–MII equilibrium expressed as the molar ratio of [MII]/[MI]; k_i, individual rate constant; k_{app}, apparent rate constant of MII formation; ΔE_a, activation energy of MII formation; OG, *n*-octyl β-D-glucopyranoside.

tion structure (*18*) is often used as a model for other GPCRs. Absorption of a photon by the 11-*cis*-retinal chromophore initiates a rapid cascade of photointermediate states which culminates after about 1 ms in a quasi-stable equilibrium between two distinct conformational states: metarhodopsin I (MI) and metarhodopsin II (MII). MII is the functionally active conformation which binds and activates transducin, G_t, the G protein involved in visual signal transduction. MI and MII have unique, well-separated absorption spectra; λ_{max} = 480 nm for MI and λ_{max} = 380 nm for MII. The spectroscopic difference between MI and MII forms the basis of assaying the activity of rhodopsin. A wealth of information has been accumulated from studies using rhodopsin-containing proteoliposomes (*10, 19−22*), yet structural and functional comparisons among these preparations are not available.

We prepared rhodopsin-containing proteoliposomes using OG and the DD and RD techniques and determined the activity of rhodopsin in terms of the MI−MII equilibrium constant, K_{eq}, and the rates of MII formation. Our results showed that the activity of rhodopsin is significantly higher in proteoliposomes prepared by the RD technique. The DD technique produced larger, more heterogeneous vesicles, while the RD technique yielded smaller and homogeneous vesicles. The DD technique produced both proteoliposomes and lipid vesicles containing no protein. The L/P ratio in the final proteoliposomes is significantly lower than that in the starting mixture. The RD technique produced proteoliposomes only, and the L/P ratio remains identical to that in the starting materials. In summary, the RD technique exhibits obvious advantages in controlling the L/P ratio and promoting rhodopsin activity.

EXPERIMENTAL PROCEDURES

Materials. Asolectin was purchased from Sigma (St. Louis, MO); concanavalin A Sepharose was from Amersham Biosciences (Piscataway, NJ); frozen bovine retinas were from James and Wanda Lawson (Lincoln, NE); *n*-octyl β-D-glucopyranoside (OG) was from EMD Chemicals, Inc. (San Diego, CA). The buffer used for proteoliposome preparation and functional studies contained 10 mM PIPES, 30 mM NaCl, 60 mM KCl, and 50 μM diethylenetriaminepentaacetic acid at pH 7.0 (PBS buffer).

Rod outer segments (ROS) were isolated from frozen bovine retinas using the modified Shake-ate method (*23*). ROS disks were prepared using the Ficoll flotation method by Smith and Litman (*24*). The isolated ROS were solublized in 30 mM OG and applied to a concanavalin A affinity column for rhodopsin purification (*25*). The column-purified rhodopsin had a 280/500 absorbance ratio of 1.8 to 1.9 and was essentially free of lipids (<0.5 lipid per rhodopsin) based on protein assay using the Lowry method (*26*) and/or ΔA_{500} of rhodopsin (*27*) and phosphate assay of phospholipid (*28*).

Rhodopsin/Asolectin Proteoliposome Preparation. Column-purified rhodopsin was mixed with OG-solublized asolectin in the dark at 4 °C and incubated for a minimum of 4 h to form mixed micelles consisting of rhodopsin, asolectin, and OG. The rhodopsin concentration in the mixed micelles was kept constant at 1 mg/mL, while the asolectin concentration was varied according to the given L/P ratio. In this study, a set of sample mixtures with low L/P ratio (molar ratio of 60:1) and high L/P ratio (molar ratio of 300:1) were used

for the preparation of proteoliposomes using the RD and DD techniques. The OG concentrations in the mixed micelles for the low and high L/P samples were 50 and 100 mM, respectively, which corresponds to a free micellar detergent-to-lipid ratio of ∼10 in both samples. Such condition is well above the complete solublization of rhodopsin and asolectin in OG (*20*).

Both the low and high L/P mixtures were split in two halves to prepare proteoliposomes in parallel using the DD and RD techniques. Half of the low and high L/P samples were dialyzed directly against PBS buffer producing DD vesicles (*20, 22*). The other half were dripped into PBS buffer so that the OG concentration was instantaneously lowered to 10 mM (well below the cmc of OG of 20 mM), which produced RD vesicles. The remaining monomeric OG was removed by further dialysis against PBS buffer (*21*). The dialysis step for both methods was carried out in 100-fold excess PBS buffer containing Bio-Beads (Bio-Rad, CA) for 36 h with three buffer exchanges (the total dilution factor is 1000000-fold). The L/P of the final proteoliposomes were determined using protein assay (*27*) and phosphate assay (*28*).

ROS Disk Vesicle Preparation. ROS disks containing 1 mg/mL rhodopsin were solublized in 50 mM OG and incubated in the dark at 4 °C for 4 h. The sample was centrifuged at 15000 rpm for 30 min in an SS34 rotor to remove any insoluble materials. The supernatant, which contains solublized ROS disks in OG, was divided in two halves for preparation of proteoliposomes using the DD and RD techniques as described above.

Equilibrium Spectra of MI−MII. The equilibrium spectra of MI−MII followed by the light activation of rhodopsin were determined at 37 °C in pH 7.0 PBS buffer as previously described (*29*). Briefly, 130 μL of proteoliposomes in PBS buffer, pH 7, was added into a microcuvette and incubated in the dark at 37 °C for 5 min. A set of four absorption spectra were collected sequentially in an Agilent 8453 diode array spectrophotometer, which consisted of the spectrum of (1) the dark-adapted rhodopsin, (2) 3 s after partially bleached rhodopsin (∼20% bleaching) by a green flash (520 ± 20 nm), (3) 10 min after the addition of 30 mM hydroxylamine into the partially bleached rhodopsin to convert bleached rhodopsin into opsin and retinal oxime, and (4) fully bleached rhodopsin by an external light for 3 min. The spectra were analyzed using a nonlinear least-squares method according to Mitchell et al. (*29*). The equilibrium constant is expressed as K_{eq} = [MII]/[MI].

Kinetics of MII Formation. The kinetics of MII formation was measured by flash photolysis in an LKS60 spectrophotometer (Applied Photophysics, Leatherhead, U.K.). An actinic flash (∼7 ns in duration) was provided by a Nd:YAG laser (Surelite I; Continuum, Santa Clara, CA) frequency doubled to 532 nm. Changes in photomultipier tube output were acquired by a 600 MHz Infiniium digital oscilloscope (Agilent Technologies, Santa Clara, CA), which has a temporal resolution of 2 ns. A microcuvette containing 130 μL of proteoliposomes with 0.2−0.3 mg/mL rhodopsin was incubated in a temperature-regulated sample holder at a set temperature for 5 min. The 0% transmission level (baseline signal) and 100% transmission level were determined prior to the activation of rhodopsin by a laser flash. The increase in absorbance at 380 nm, which is the absorption maximum
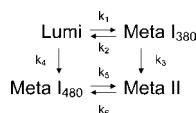
FIGURE 1: Square model of the rhodopsin photoreaction cascade from lumirhodopsin (Lumi) to metarhodopsin II (Meta II) (*30, 31*).

of MII, induced by a single laser flash was monitored until completion of the reaction. The signal was differentially amplified and recorded by the digital oscilloscope in an oversampling mode, which collects 32000 data points per trace. The data were reduced to 2000 points using boxcar averaging. The vendor software !Laser (Applied Photophysics, Leatherhead, U.K.) allocates 10% of the points as pretrigger data points, which were used to convert the voltage signal into absorbance. The transient absorbance was calculated as $\Delta A = \log VA/VA'$, where VA is the voltage of the pretrigger data and VA' is the voltage of the transient signal. Samples were measured in a minimum of triplet, and the transient absorption traces were averaged. The transient absorbance at 380 nm was analyzed using two separate methods: (1) Sum of three exponentials, $\Delta A = C_0\sum_{i=1}^{3}f_i(1 - \exp(-k_it))$, where C_0 is the magnitude of the transient absorbance at equilibrium and f_i is the fraction of the kinetic process occurring with rate k_i. The apparent rate constant of MII formation, $k_{app}(380)$, is calculated as $\ln k_{app}(380) = \sum_{i=1}^{3}f_i \ln k_i$, where f_i and k_i are the same as above. (2) The square decay model, shown in Figure 1 (*30, 31*), and the best-fit values of the six microscopic rate constants were determined directly via analysis with NONLIN using a subroutine specifying the solution of the coupled differential equations of the square model written by the authors. The small contribution of the MI species to the observed absorbance increase at 380 nm was determined from analysis of spectra of equilibrium mixtures of MI and MII. $k_{app}(MII)$ is calculated as the inverse of the time required for MII to rise to $1 - 1/e$ of its final plateau value.

Isopycnic Gradient Centrifugation. One milliliter of each vesicle preparation was layered on the top of a 10 mL continuous sucrose gradient (0–50% w/w) and centrifuged in an SW-41 rotor at 30000 rpm (154000*g*) overnight. The gradient was fractionated in 0.5 mL aliquots from the bottom of the tube to the top. The sucrose concentration of each fraction was analyzed using a refractometer, the protein content was determined by Lowry assay and ΔA_{500} assay (*27*), and the lipid concentration was determined via phosphate assay (*28*).

Electron Microscopy Imaging. Negative staining electron microscopy was performed following the protocol of Palmer et al. (*32*). Briefly, each proteoliposome sample was adsorbed on a Formvar carbon-coated grid, which was glow-discharged in a vacuum evaporator (Edward, Wilmington, MA) prior to use (*33*). The grid was stained with 1% PTA (phosphotungstic acid, pH 7.0); excess solution was blotted and allowed to air-dry. The grid was examined and imaged using a Hitachi H7600 electron microscope (Tokyo, Japan) equipped with an AMT digital camera (Danvers, MA).

RESULTS

Effect on the Equilibrium of MI–MII Formation. The activity of rhodopsin is preserved in proteoliposomes pre-
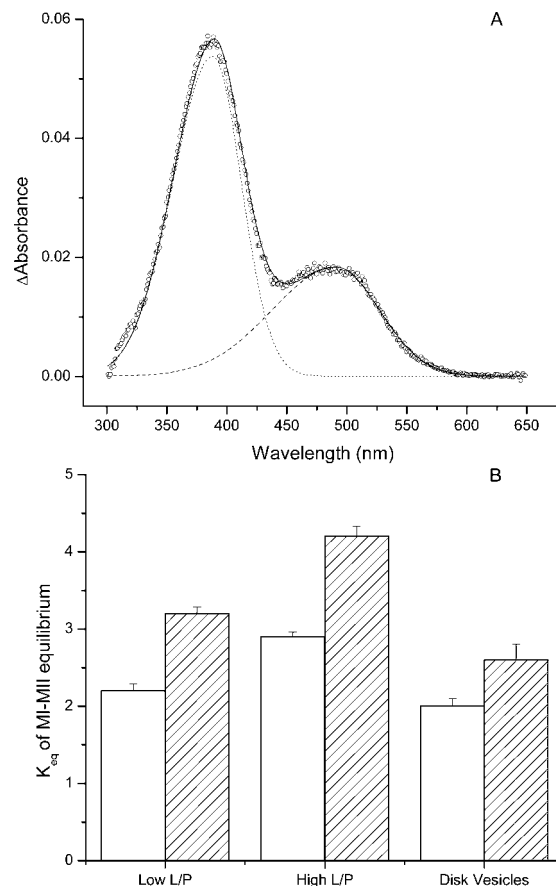

FIGURE 2: Equilibrium UV/vis measurement of MII formation. Panel A: An example of the equilibrium spectrum of MI and MII in the RD vesicles with L/P ratio at 37 °C in pH 7.0 PBS buffer. The open circles represent the equilibrium spectrum of MI and MII derived from a series of UV/vis spectra as described in the Experimental Procedures. The dotted curve is the deconvolved absorption spectrum of MII with a maximum at 380 nm; the dashed curve is the deconvolved absorption spectrum of MI with a maximum at 480 nm. The solid curve is the sum of the deconvolved spectra of MI and MII. Panel B: Summary of K_{eq} of MI and MII equilibrium in various vesicles at 37 °C in pH 7.0 PBS buffer. The DD preparations are shown in open bars; the RD preparations are shown in hatched bars.

pared by the RD and DD techniques. Both MI and MII photointermediates were formed upon light activation of rhodopsin (Figure 2A). The wavelengths of maximum absorption and band shapes of the MI and MII absorption bands were essentially identical in all proteoliposomes at all temperatures. However, the relative peak intensities of MI and MII varied among different proteoliposomes. Among the three groups of proteoliposomes prepared in this study, which are rhodopsin in asolectin with low and high L/P ratios and disk vesicles, the K_{eq} values are consistently higher in RD vesicles than in DD vesicles (Figure 2B). The RD vesicles exhibited 30–45% higher K_{eq} values compared to the corresponding DD vesicles. The high L/P asolectin group overall has the highest K_{eq} values, while the low L/P group and the disk vesicle group have comparable K_{eq} values.

Effect on the Kinetics of MII Formation. The activation of rhodopsin by a laser flash resulted in a rapid increase of absorbance at 380 nm corresponding to formation of the MII species for all proteoliposomes. However, the rate of the transient absorbance varied substantially between RD and DD vesicles. Shown in Figure 3A are examples of transient absorbance traces acquired from the high L/P group at 37
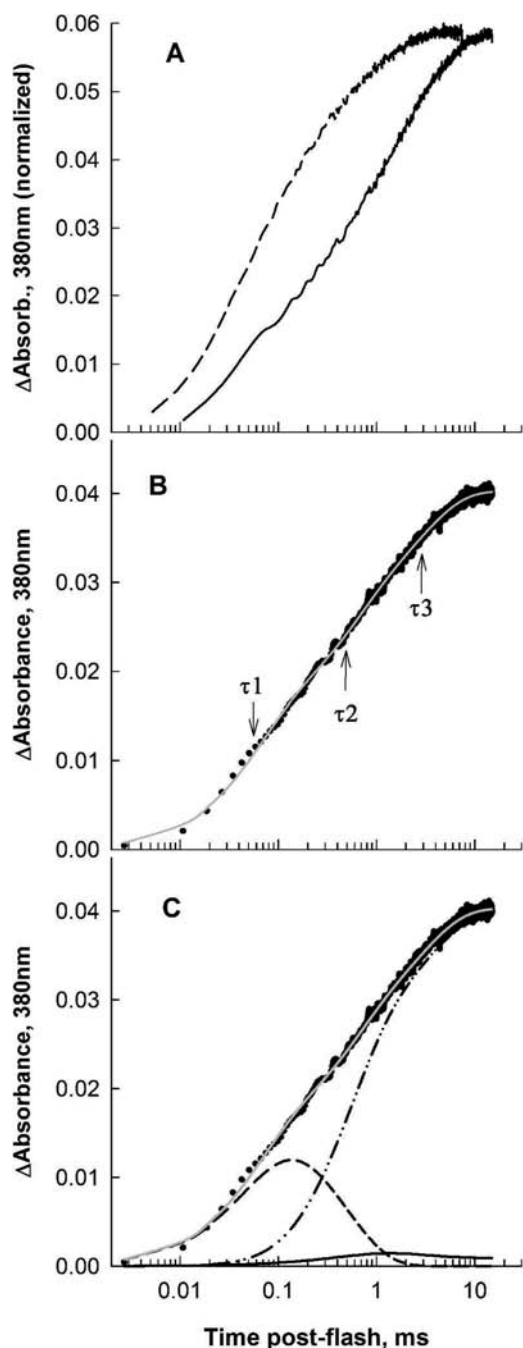
FIGURE 3: Transient absorption of MII formation obtained at 380 nm via laser flash photolysis at 37 °C. Transient absorbance initiated by laser flash was collected from time zero until reaching a plateau. (A) Typical transient absorbance traces of MII formation from proteoliposomes with high L/P ratios prepared by the RD (dash curve) and DD techniques (solid curve). Traces have been scaled to the same maximum absorbance change to emphasize the differences in kinetics. (B) An example of analyzing the transient absorbance using the sum-of-three exponential model. The dotted curve is the transient absorbance at 380 nm from the high L/P DD sample (the solid curve in curve in panel A); the white line is the fitted curve according to the sum-of-three exponential equation. τ_1, τ_2, and τ_3 are the individual time constants derived from the three exponentials, which are expressed as $1/k_i$ from Table 1. (C) An example of analyzing the transient absorbance in terms of the square model (Figure 1). The dotted trace is the same as the solid curve in panel A. The three postlumi species and their sum are shown by the smooth curves; the dash curve is MI-380, the black curve is MI-480, the dash-dotted curve is MII, and the white curve is the total fit, which is the sum of MI-380, MI-480, and MII.

°C. The amplitude of the traces is normalized to the same plateau value to facilitate the comparison of the kinetic process. The transient absorbance of photoactivated rhodopsin in the RD vesicles rises at an earlier time scale than that of DD vesicles, indicating the formation of MII is faster in RD vesicles. The same trend was observed in each group of vesicles measured at 25, 30, and 37 °C. This demonstrates that the activity of rhodopsin, expressed in terms of the rate of MII formation, is higher in RD vesicles than in DD vesicles, which is consistent with the observations from the equilibrium measurements.

Empirical description of the transient absorbance of MII formation required the sum-of-three exponential functions (Figure 3B), consistent with previous reports (*29, 34*). A sum-of-two exponentials was insufficient to fit the data based on the fitting residuals and variance of fit, while a sum-of-four exponentials produced no significant improvement in variance of fit (data not shown).

The flash-induced transient increase in absorbance at 380 nm was also analyzed in terms of the square model shown in Figure 1, which is based on a series of multiwavelength flash photolysis studies (*30, 31*). A key feature of this model is that the observed absorbance increase at 380 nm is considered to be the sum of three distinct photointermediate species. The contributions of these three species are evident in the deconvoluted kinetic trace shown in Figure 3C. The initial absorbance increase is due to MI-380 (dash curve), which reaches a maximum at between 100 and 200 μs. Over the first $\sim$200 μs MII (dash-dotted curve) is a minor contributor to the observed absorbance increase, but this changes as MI-380 decays away, and after 2 to 3 ms the absorbance increase is due to MII plus a small contribution from MI-480 (black curve). The quality of the square model analysis is reflected in the values of the standard deviations for the derived microscopic rate constants, which were generally less than 10% of each rate constant. NONLIN returns uncertainties corresponding to 1 standard deviation above and below the best-fit value for each parameter. The high and low standard deviations generally differed by less than 10%; thus the average standard deviation is reported. Analysis in terms of the square model requires optimization of six microscopic rate constants, meaning it is mathematically equivalent to analysis with the sum-of-three exponentials model, which also has six independent parameters. Thus, the variances of the final fits obtained with the two analytical models were identical in all cases.

In order to compare MII kinetics between the different proteoliposomes in terms of a single parameter, we derived the apparent rate constant of MII formation from the three-exponential analysis and square model analysis: $k_{app}(380)$ from the three-exponential analysis is calculated as a weighted average of the natural logarithm of the individual rate constants, as described in the Experimental Procedures section; $k_{app}(MII)$ was determined from the analytical solution of MII as a function of time, as shown by the dash-dotted curve in the example in Figure 3C. Final values were determined by NONLIN, following determination of the microscopic rate constants, so that uncertainties in all rate constants were propagated to obtain the correct uncertainty in $k_{app}(MII)$. The results from the three-exponential analysis and square model analysis are summarized in Tables 1 and 2, respectively.

Table 1: Summary of the Laser Flash Photolysis Measurement of Rhodopsin Activation Analyzed by a Sum-of-Three Exponential Function[a]

sample	T (°C)	C_0	f_1	k_1	f_2	k_2	f_3	k_3	$k_{app}(380)$
DD (low L/P)	25	0.041 (0.00)	0.62 (0.03)	0.037 (0.003)	0.23 (0.02)	0.23 (0.04)	0.15 (0.01)	3.88 (0.84)	0.11 (0.01)
	30	0.045 (0.00)	0.38 (0.02)	0.068 (0.013)	0.41 (0.02)	0.43 (0.02)	0.21 (0.01)	5.4 (0.8)	0.36 (0.03)
	37	0.052 (0.00)	0.45 (0.03)	0.26 (0.02)	0.32 (0.03)	1.48 (0.32)	0.23 (0.03)	19.20 (4.77)	1.21 (0.07)
RD (low L/P)	25	0.034 (0.00)	0.43 (0.02)	0.027 (0.001)	0.33 (0.01)	0.13 (0.01)	0.24 (0.01)	2.10 (0.14)	0.13 (0.01)
	30	0.037 (0.00)	0.47 (0.03)	0.071 (0.005)	0.30 (0.02)	0.36 (0.06)	0.23 (0.01)	5.45 (0.88)	0.31 (0.01)
	37	0.040 (0.00)	0.47 (0.02)	0.36 (0.02)	0.25 (0.01)	1.77 (0.24)	0.28 (0.01)	17.25 (1.18)	1.59 (0.04)
DD (high L/P)	25	0.047 (0.00)	0.54 (0.01)	0.065 (0.002)	0.22 (0.01)	0.36 (0.04)	0.24 (0.01)	3.86 (0.23)	0.25 (0.00)
	30	0.055 (0.00)	0.47 (0.01)	0.13 (0.00)	0.27 (0.01)	0.86 (0.07)	0.26 (0.01)	8.80 (0.58)	0.66 (0.00)
	37	0.059 (0.00)	0.35 (0.02)	0.35 (0.02)	0.29 (0.02)	2.04 (0.27)	0.36 (0.02)	17.78 (1.43)	2.40 (0.02)
RD (high L/P)	25	0.065 (0.00)	0.36 (0.01)	0.14 (0.01)	0.34 (0.01)	0.81 (0.05)	0.30 (0.01)	6.76 (0.34)	0.82 (0.01)
	30	0.065 (0.00)	0.31 (0.01)	0.33 (0.01)	0.34 (0.01)	1.96 (0.02)	0.35 (0.02)	12.88 (0.83)	2.17 (0.03)
	37	0.070 (0.00)	0.23 (0.01)	0.97 (0.03)	0.32 (0.02)	5.39 (0.06)	0.45 (0.03)	26.56 (2.53)	7.45 (0.08)
DD (disk vesicles)	25	0.047 (0.00)	0.38 (0.01)	0.05 (0.00)	0.46 (0.01)	0.29 (0.01)	0.16 (0.01)	2.52 (0.18)	0.22 (0.01)
	30	0.045 (0.00)	0.40 (0.01)	0.13 (0.00)	0.41 (0.01)	0.75 (0.03)	0.18 (0.01)	5.04 (0.30)	0.52 (0.01)
	37	0.048 (0.00)	0.43 (0.01)	0.49 (0.02)	0.40 (0.01)	3.07 (0.17)	0.18 (0.01)	24.48 (2.33)	2.05 (0.08)
RD (disk vesicles)	25	0.047 (0.00)	0.57 (0.01)	0.20 (0.00)	0.33 (0.01)	0.98 (0.03)	0.11 (0.00)	10.06 (0.50)	0.51 (0.01)
	30	0.047 (0.00)	0.40 (0.01)	0.34 (0.01)	0.42 (0.01)	1.42 (0.04)	0.18 (0.00)	10.98 (0.40)	1.15 (0.02)
	37	0.047 (0.00)	0.28 (0.02)	0.89 (0.06)	0.46 (0.02)	3.59 (0.20)	0.25 (0.01)	23.69 (1.05)	3.89 (0.17)

[a] The individual rate constant is expressed in ms^{-1}. $\Delta A = C_0 \sum_{i=1}^{3} f_i (1 - \exp(-k_i t))$, where C_0 is the amplitude of the absorbance change, f_i is the fraction of the individual exponential term k_i, and k_i is the individual rate constant. Numbers in parentheses are 1 standard deviation.

Table 2: Summary of the Laser Flash Photolysis Measurement of Rhodopsin Activation Analyzed by the Square Model (Figure 1)[a]

proteoliposome	T (°C)	k_1	k_2	k_3	k_4	k_5	k_6	$k_{app}(MII)$
DD (low L/P)	25	0.27 (0.02)	1.67 (0.14)	0.29 (0.02)	0.11 (0.01)	0.018 (0.001)	0.017 (0.001)	0.056 (0.001)
	30	0.75 (0.06)	3.79 (0.48)	0.70 (0.06)	0.21 (0.02)	0.038 (0.001)	0.027 (0.001)	0.13 (0.002)
	37	3.40 (0.37)	12.98 (2.50)	3.27 (0.52)	1.07 (0.15)	0.17 (0.01)	0.086 (0.004)	0.59 (0.02)
RD (low L/P)	25	0.34 (0.02)	1.50 (0.10)	0.29 (0.02)	0.09 (0.01)	0.016 (0.001)	0.011 (0.001)	0.058 (0.001)
	30	1.00 (0.09)	3.75 (0.49)	0.79 (0.09)	0.25 (0.01)	0.050 (0.002)	0.021 (0.001)	0.15 (0.004)
	37	4.12 (0.16)	10.37 (0.73)	3.26 (0.32)	1.25 (0.15)	0.27 (0.01)	0.090 (0.003)	0.75 (0.02)
DD (high L/P)	25	0.61 (0.02)	2.66 (0.17)	0.64 (0.05)	0.30 (0.03)	0.037 (0.001)	0.028 (0.001)	0.12 (0.002)
	30	1.70 (0.06)	5.70 (0.41)	1.61 (0.13)	0.66 (0.05)	0.087 (0.002)	0.047 (0.001)	0.30 (0.006)
	37	5.39 (0.23)	9.65 (0.82)	3.43 (0.44)	1.36 (0.17)	0.26 (0.01)	0.086 (0.005)	1.02 (0.07)
RD (high L/P)	25	1.68 (0.04)	3.80 (0.23)	1.55 (0.11)	0.53 (0.04)	0.102 (0.003)	0.040 (0.002)	0.40 (0.01)
	30	4.02 (0.10)	6.22 (0.42)	3.40 (0.32)	1.20 (0.10)	0.25 (0.01)	0.077 (0.003)	1.04 (0.05)
	37	11.32 (0.25)	9.63 (0.64)	8.06 (1.03)	2.94 (0.31)	0.80 (0.04)	0.18 (0.01)	3.23 (0.27)
DD (disk vesicles)	25	0.31 (0.02)	1.12 (0.20)	0.66 (0.10)	0.17 (0.02)	0.03 (0.00)	0.02 (0.00)	0.13 (0.00)
	30	0.72 (0.04)	1.85 (0.31)	1.17 (0.22)	0.37 (0.06)	0.07 (0.01)	0.04 (0.00)	0.29 (0.02)
	37	3.78 (0.29)	12.83 (2.81)	6.91 (1.28)	1.95 (0.24)	0.32 (0.02)	0.16 (0.01)	1.18 (0.03)
RD (disk vesicles)	25	0.94 (0.04)	5.16 (0.61)	2.70 (0.23)	0.61 (0.05)	0.13 (0.01)	0.06 (0.02)	0.32 (0.00)
	30	1.82 (0.06)	5.70 (0.60)	3.65 (0.34)	0.87 (0.07)	0.23 (0.01)	0.10 (0.00)	0.70 (0.01)
	37	5.70 (0.21)	11.39 (1.27)	8.17 (1.21)	2.15 (0.34)	0.69 (0.06)	0.26 (0.02)	2.18 (0.07)

[a] The individual rate constant is expressed in ms^{-1}. Numbers in parentheses are 1 standard deviation.

Figure 4 shows an example of the apparent rate constant of MII formation, $k_{app}(380)$ (panel A) and $k_{app}(MII)$ (panel B), in the three groups of proteoliposomes at 37 °C. The value of $k_{app}(MII)$ is smaller than that of $k_{app}(380)$ since the square model assigns the initial absorbance increase at 380 nm to the formation of MI-380. However, both panels gave similar patterns of apparent rate constants between the RD and DD vesicles. The apparent rate constant of MII formation is consistently higher in RD vesicles than in DD vesicles. The ratios of $k_{app}(380)$ between RD and DD vesicles in the low L/P vesicles, high L/P vesicles, and disk vesicles are 1.3, 3.1, and 1.9, respectively. Similar ratios of $k_{app}(MII)$ were observed between these vesicles, which are 1.5, 3.2, and 1.8, respectively. The highest apparent rate constant was observed in RD vesicles with high L/P ratio, while the lowest one was observed in DD vesicles with low L/P ratio.

The temperature dependence of $k_{app}(380)$ and $k_{app}(MII)$ was examined in terms of the Arrhenius equation as shown in Figure 5. Both methods of analysis yielded a straight line for each preparation of proteoliposomes, predicted from the Arrhenius equation. The lines associated with RD vesicles in each group are located above those from DD vesicles, again demonstrating that the rate of MII formation is higher in the RD preparations. The activation energies derived from the Arrhenius plot are summarized in Table 3. The activation energies of rhodopsin activation derived from $k_{app}(380)$ and $k_{app}(MII)$ are comparable to each other. No clear difference of E_a is observed between the RD and DD preparations. The E_a values are slightly higher in the low L/P group compared to the high L/P.

Physical Characterization of DD and RD Vesicles. Previous studies have demonstrated that the proteoliposomes prepared by DD and RD techniques have several different physical characteristics, such as morphology, vesicle size, and L/P ratios (*20, 21*). These differences were confirmed in the present study. DD vesicles have a higher level of light scattering, indicating larger vesicle sizes (data not shown). Electron microscopic imaging demonstrates that DD vesicles are more heterogeneous and have a broader distribution of vesicle sizes, while the RD vesicles are more homogeneous. The average sizes of vesicle diameters of DD and RD vesicles were 109 ± 54 and 53 ± 12 nm, respectively.

The distribution profiles of DD and RD vesicles in the sucrose gradient (0−50%) were strikingly different. RD vesicles yielded one tight band in the sucrose gradient. The location of the band is dependent on the L/P ratio in the
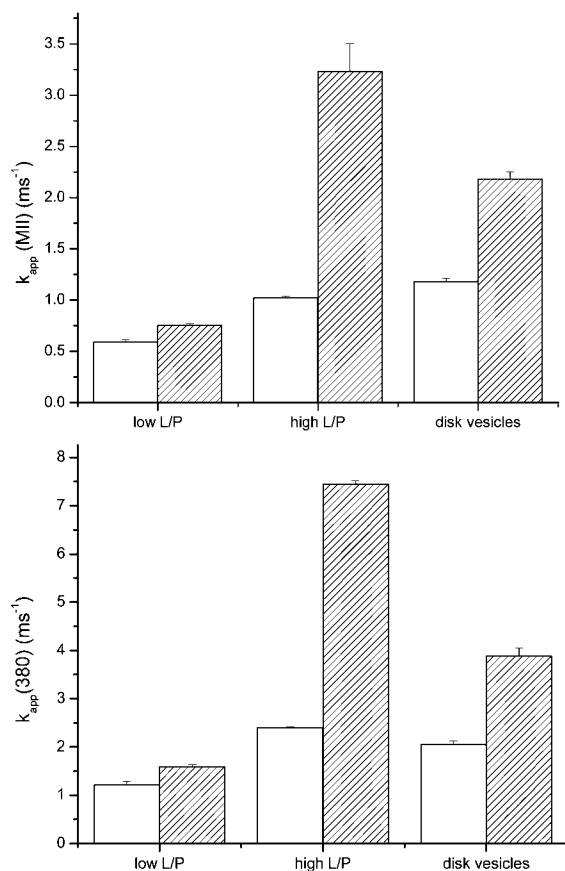
FIGURE 4: Summary of the apparent rate constants of MII formation at 37 °C derived from the sum-of-three exponential analysis (panel A, top) and square model analysis (panel B, bottom). The DD vesicles are shown in open bars; the RD vesicles are shown in hatched bars.
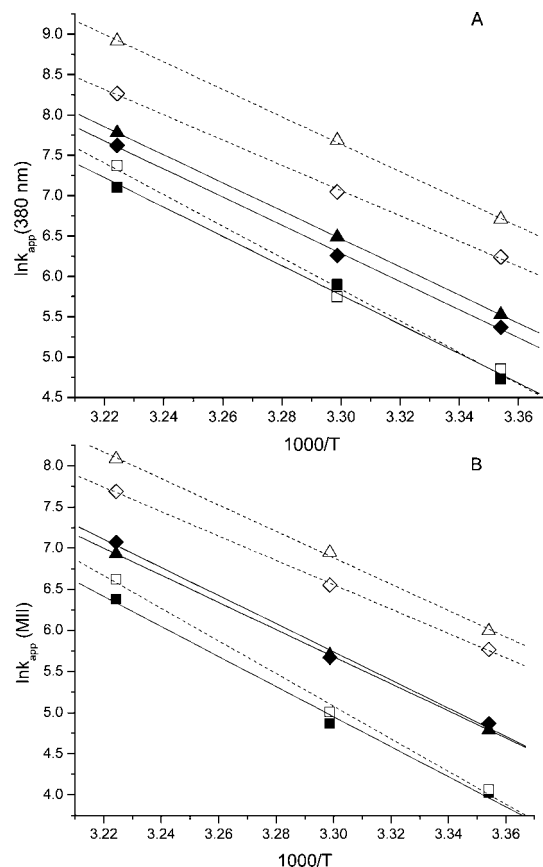

FIGURE 5: Arrhenius plot of the apparent rate constant of MII formation derived from the sum-of-three exponential analysis (panel A) and square model analysis (panel B). The samples are low L/P DD vesicles (■), low L/P RD vesicles (□), high L/P DD vesicles (▲), high L/P RD vesicles (△), DD disk vesicles (◆), and RD disk vesicles (◇). Dash lines are linear fits of the RD samples; solid lines are linear fits of the DD samples.

Table 3: Activation Energies (kJ/mol) Associated with the Apparent Rate of MII Formation Derived from the Three-Exponential Model (k_{app}(380)) and Square Model (k_{app}(MII))[a]

sample	E_a (k_{app}(380))	E_a (k_{app}(MII))
DD (low L/P)	151.4 (11.1)	151.9 (11.9)
RD (low L/P)	161.8 (13.3)	164.9 (10.4)
DD (high L/P)	144.4 (1.3)	137.1 (0.3)
RD (high L/P)	141.6 (3.1)	133.4 (4.9)
DD (disk vesicles)	144.5 (4.6)	142.9 (9.9)
RD (disk vesicles)	129.9 (3.6)	123.2 (2.1)

[a] Numbers in parentheses are 1 standard deviation.

initial mixture. In the low L/P preparation, the band was located at 35−40% sucrose (1.16−1.18 g/mL), while in the high L/P preparation it appeared at 17−22% sucrose (1.07−1.09 g/mL). Both phospholipids and rhodopsin are detected in these vesicles, indicating the formation of true proteoliposomes in the RD preparation. On the other hand, DD vesicles yielded two visible bands in the sucrose gradient. The top band was located at 10−15% sucrose (1.04−1.06 g/mL), which has identical density to the pure lipid vesicles, while the bottom band was at 30−40% sucrose (1.13−1.18 g/mL) and has a density similar to that of native disk membranes. The high-density band is much broader, indicating more heterogeneity in sample composition. The positions of these bands remain unchanged when the L/P ratios were changed in the initial mixtures. Protein and lipid analysis of these fractions confirmed that the low-density band contained only phospholipids, while the high-density band contained both phospholipids and rhodopsin. This demonstrates that the dialysis method produced both proteoliposomes and nonproteoliposomes.

The L/P ratios in the final proteoliposomes produced by DD and RD differed significantly. The L/P ratios in the low L/P vesicles, high L/P vesicles, and disk vesicles produced by the RD technique are 58 ± 5, 338 ± 41, and 73 ± 5, respectively, similar to those in the initial mixtures, while the corresponding ratios in DD vesicles are 54 ± 3, 67 ± 4, and 47 ± 3, which is significantly lower. Similar findings were reported from a previous study (*20, 21*). This result demonstrates that the L/P ratios in the final proteoliposomes

in the RD preparation are similar to those in the initial mixtures. Therefore, the L/P ratios in RD vesicles can be easily controlled by changing the L/P ratio in the initial mixture. However, the L/P ratios in the DD preparation had a narrow range of variation and are difficult to be manipulated.

DISCUSSION

When properly constructed, proteoliposome can be used as a valuable tool to tackle the complexity of biomembranes and as an effective venue to study lipid−protein and protein−protein interactions in a simplified and well-defined membrane environment. Much of our current understanding on the structure and function of biomembranes is derived from studies using proteoliposomes (*3−15*). Many procedures have been developed for the preparation of proteoli-

posomes. Though the physical characteristics of various preparations of proteoliposomes have been described previously (*13, 20, 21*), the effect of different preparations on the function of membrane proteins is rarely addressed. In this study, we observed that different procedures of preparing proteoliposomes can have significant influence on protein function. We demonstrated that rhodopsin is more active in proteoliposomes prepared by the RD procedure. K_{eq} of the MI−MII equilibrium is 30−45% higher in RD vesicles than in DD vesicles, and the apparent rate of MII formation is as much as 3-fold faster in RD vesicles. A higher value of K_{eq} corresponds to an increase concentration of the enzymatically active MII conformation being formed during the light activation of rhodopsin, while a higher rate constant of MII formation indicates a quicker formation of this active conformational state. Both are important functional parameters for the activation of rhodopsin and its subsequent activation of the visual cascade. A higher yield of MII formation indicates a higher visual sensitivity, while a higher rate of MII formation corresponds to a quicker response time for visual transduction. Preserving the optimal protein function is often a desirable objective for preparing proteoliposomes. In such cases, the RD technique appears to have a clear advantage over the DD technique.

One major structural difference between RDV and DDV is the L/P ratio in the final proteoliposomes. The proteoliposomes prepared by the RD procedure have identical L/P ratio to that in the initial mixture. This is consistent with observations in other studies (*21, 35, 36*). Using this procedure, we were able to prepare proteoliposomes with L/P ratio up to 10000 to 1. The DD technique, on the other hand, produced proteoliposomes with lower L/P ratio than that in the initial mixture. The L/P ratios in the final proteoliposomes prepared by the DD technique are between 47 and 67 despite much higher L/P ratios in the initial mixture. A similar L/P ratio of 48−61 was observed in rhodopsin-containing vesicles in several unsaturated phosphatidylcholines prepared by the DD technique, even though the L/P ratio as high as 300 to1 is used in the initial mixture (*20*).

The RD procedure has an obvious advantage if a controlled L/P ratio is required in the final proteoliposomes, such as to study lipid−protein and protein−protein interactions as a function of the surface density of membrane protein. A narrow range of L/P ratio in proteoliposomes prepared by the DD technique could limit its broad applications in such scenarios. Currently, there is an intense debate on the topic of rhodopsin dimerization (*37−40*), which is related to a more general topic of GPCR dimerization (*41−44*). Rhodopsin-containing proteoliposomes have been applied in characterizing rhodopsin−rhodopsin interactions recently (*39, 40*). However, a broader range of L/P ratios, which could be achieved if the RD technique is used, would provide a more unambiguous answer to whether rhodopsin exists as monomer or dimer.

One study reported that the proteoliposomes produced by the DD technique retained the asymmetric orientation of rhodopsin in membranes (*22*), which could be a major advantage of the DD technique. Most other proteoliposome preparations resulted in a random orientation of proteins in membranes, resulting in half of the proteins oriented in the opposite side of the membranes.

The higher L/P ratio in proteoliposomes prepared by the RD technique is likely the main contributing factor to the higher level of rhodopsin activity in RD vesicles. In a previous study we demonstrated the L/P ratio in proteoliposomes has a direct correlation with the equilibrium concentration of MII formation (*36*). In a separate experiment, we determined kinetics of MII formation in a series of rhodopsin/18:0,18:1PC proteoliposomes with L/P ratio of 100, 250, and 1000, prepared by the RD technique. The apparent rate constants of MII formation at 25 °C were 1.1, 3.4, and 4.1 ms^{-1}, respectively. This demonstrates that the rate of MII formation directly correlates with the L/P ratios in proteoliposomes. Among all proteoliposomes prepared in this study, the same correlation was observed between the apparent rate constants of MII formation and L/P ratios, suggesting the difference in L/P ratio between the RD and DD preparations is likely responsible for the difference in rhodopsin activity. A recent study by solid-state NMR demonstrated that the formation of MII is accompanied by a significant conformational change involving the tilting and inward motion of helix 6 (*45*). Proteoliposomes with higher L/P ratios have lower surface density of rhodopsin in lipid membranes, which have less restriction on the conformational change of rhodopsin from the neighboring molecules during photoactivation; therefore, a higher level of rhodopsin activity is expected.

Additional factors may also contribute to the functional difference between the RD and DD preparations, since the L/P ratios between the RD and DD preparations in the low L/P group only differed slightly (58 vs 54), yet significant differences of K_{eq} and k_{app} were observed among these samples. The diameters of DD and RD vesicles were 109 ± 54 and 53 ± 12 nm, respectively; thus the difference in membrane curvature may play a role in the observed differences in rhodopsin function in the low L/P regime. Rhodopsin in the more highly curved RD vesicles formed MII at a faster rate (Tables 1 and 2) and had a higher concentration of MII at equilibrium (Figure 2). This difference is consistent with the flexible surface model of rhodopsin−bilayer interaction which describes how membrane curvature enhances MII formation (*40, 46*).

In summary, this study demonstrates that proteoliposomes prepared by different techniques have a profound impact on the activity level of a membrane protein as well as the physical characteristics of the final proteoliposomes. Overall, this work suggests that the RD technique has advantages over the DD technique in terms of preserving optimal rhodopsin activity and controlling L/P ratio in the final proteoliposomes.

ACKNOWLEDGMENT

REFERENCES

1. Wallin, E., and von Heijne, G. (1998) Genome-wide analysis of integral membrane proteins from eubacterial, archaean, and eukaryotic organisms. *Protein Sci. 7*, 1029–1038.
2. Jones, D. T. (1998) Do transmembrane protein superfolds exist? *FEBS Lett. 423*, 281–285.
3. Sharom, F. J. (1995) Characterization and functional reconstitution of the multidrug transporter. *J. Bioenerg. Biomembr. 27*, 15–22.

4. McNamee, M. G., and Ochoa, E. L. (1982) Reconstitution of acetylcholine receptor function in model membranes. *Neuroscience* 7, 2305–2319.

5. Montal, M. (1987) Reconstitution of channel proteins from excitable cells in planar lipid bilayer membranes. *J. Membr. Biol. 98*, 101–115.

6. Drachev, L. A., Frolov, V. N., Kaulen, A. D., Liberman, E. A., Ostroumov, S. A., Plakunova, V. G., Semenov, A. Y., and Skulachev, V. P. (1976) Reconstitution of biological molecular generators of electric current. Bacteriorhodopsin. *J. Biol. Chem. 251*, 7059–7065.

7. Drachev, L. A., Jasaitis, A. A., Kaulen, A. D., Kondrashin, A. A., Chu, L. V., Semenov, A. Y., Severina, I. I., and Skulachev, V. P. (1976) Reconstitution of biological molecular generators of electric current. Cytochrome oxidase. *J. Biol. Chem. 251*, 7072–7076.

8. Drachev, L. A., Jasaitis, A. A., Mikelsaar, H., Nemecek, I. B., Semenov, A. Y., Semenova, E. G., Severina, I. I., and Skulachev, V. P. (1976) Reconstitution of biological molecular generators of electric current. H^+-ATPase. *J. Biol. Chem. 251*, 7077–7082.

9. Wrigglesworth, J. M., and Nicholls, P. (1979) Turnover and vectorial properties of cytochrome *c* oxidase in reconstituted vesicles. *Biochim. Biophys. Acta 547*, 36–46.

10. Hong, K., Knudsen, P. J., and Hubbell, W. L. (1982) Purification of rhodopsin on hydroxyapatite columns, detergent exchange, and recombination with phospholipids. *Methods Enzymol. 81*, 144–150.

11. Meyer, E. M., and Cooper, J. R. (1982) High-affinity choline transport in proteoliposomes derived from rat cortical synaptosomes. *Science 217*, 843–845.

12. Rigaud, J. L., Bluzat, A., and Buschlen, S. (1983) Incorporation of bacteriorhodopsin into large unilamellar liposomes by reverse phase evaporation. *Biochem. Biophys. Res. Commun. 111*, 373–382.

13. Rigaud, J. L., and Levy, D. (2003) Reconstitution of membrane proteins into liposomes. *Methods Enzymol. 372*, 65–86.

14. Silvius, J. R. (1992) Solubilization and functional reconstitution of biomembrane components. *Annu. Rev. Biophys. Biomol. Struct. 21*, 323–348.

15. Seddon, A. M., Curnow, P., and Booth, P. J. (2004) Membrane proteins, lipids and detergents: not just a soap opera. *Biochim. Biophys. Acta 1666*, 105–117.

16. Eytan, G. D. (1982) Use of liposomes for reconstitution of biological functions. *Biochim. Biophys. Acta 694*, 185–202.

17. Darszon, A., Vandenberg, C. A., Schonfeld, M., Ellisman, M. H., Spitzer, N. C., and Montal, M. (1980) Reassembly of protein-lipid complexes into large bilayer vesicles: perspectives for membrane reconstitution. *Proc. Natl. Acad. Sci. U.S.A. 77*, 239–243.

18. Palczewski, K., Kumasaka, T., Hori, T., Behnke, C. A., Motoshima, H., Fox, B. A., Le, T. I., Teller, D. C., Okada, T., Stenkamp, R. E., Yamamoto, M., and Miyano, M. (2000) Crystal structure of rhodopsin: A G protein-coupled receptor. *Science 289*, 739–745.

19. Applebury, M. L., Zuckerman, D. M., Lamola, A. A., and Jovin, T. M. (1974) Rhodopsin. Purification and recombination with phospholipids assayed by the metarhodopsin I leads to metarhodopsin II transition. *Biochemistry 13*, 3448–3458.

20. Jackson, M. L., and Litman, B. J. (1982) Rhodopsin-phospholipid reconstitution by dialysis removal of octyl glucoside. *Biochemistry 21*, 5601–5608.

21. Jackson, M. L., and Litman, B. J. (1985) Rhodopsin-egg phosphatidylcholine reconstitution by an octyl glucoside dilution procedure. *Biochim. Biophys. Acta 812*, 369–376.

22. Niu, L., Kim, J. M., and Khorana, H. G. (2002) Structure and function in rhodopsin: asymmetric reconstitution of rhodopsin in liposomes. *Proc. Natl. Acad. Sci. U.S.A. 99*, 13409–13412.

23. McDowell, J. H., and Kuhn, H. (1977) Light-induced phosphorylation of rhodopsin in cattle photoreceptor membranes: substrate activation and inactivation. *Biochemistry 16*, 4054–4060.

24. Smith, H. G., Jr., and Litman, B. J. (1982) Preparation of osmotically intact rod outer segment disks by Ficoll flotation. *Methods Enzymol. 81*, 57–61.

25. Litman, B. J. (1982) Purification of rhodopsin by concanavalin A affinity chromatography. *Methods Enzymol. 81*, 150–153.

26. Lowry, O. H., Rosebrough, N. J., Farr, A. L., and Randall, R. J. (1951) Protein measurement with the Folin phenol reagent. *J. Biol. Chem. 193*, 265–275.

27. Shichi, H. (1970) Spectrum and purity of bovine rhodopsin. *Biochemistry 9*, 1973–1977.

28. Bartlett, G. R. (1959) Phosphorus assay in column chromatography. *J. Biol. Chem. 234*, 466–468.

29. Straume, M., Mitchell, D. C., Miller, J. L., and Litman, B. J. (1990) Interconversion of metarhodopsins I and II: a branched photointermediate decay model. *Biochemistry 29*, 9135–9142.

30. Thorgeirsson, T. E., Lewis, J. W., Wallace-Williams, S. E., and Kliger, D. S. (1993) Effects of temperature on rhodopsin photointermediates from lumirhodopsin to metarhodopsin II. *Biochemistry 32*, 13861–13872.

31. Szundi, I., Lewis, J. W., and Kliger, D. S. (1997) Deriving reaction mechanisms from kinetic spectroscopy. Application to late rhodopsin intermediates. *Biophys. J. 73*, 688–702.

32. Palmer, E. L., and Martin, M. L. (1988) *Electron Microscopy in Viral Diagnosis*, CRC Press, Boca Raton, FL.

33. Hayat, M. A. (1989) *Principles and Techniques of Electron Microscopy. Biological Applications*, CRC Press, Boca Raton, FL.

34. Lewis, J. W., Winterle, J. S., Powers, M. A., Kliger, D. S., and Dratz, E. A. (1981) Kinetics of rhodopsin photolysis intermediates in retinal rod disk membranes—I. Temperature dependence of lumirhodopsin and metarhodopsin I kinetics. *Photochem. Photobiol. 34*, 375–384.

35. Polozova, A., and Litman, B. J. (2000) Cholesterol dependent recruitment of di22:6-PC by a G protein-coupled receptor into lateral domains. *Biophys. J. 79*, 2632–2643.

36. Niu, S. L., and Mitchell, D. C. (2005) Effect of packing density on rhodopsin stability and function in polyunsaturated membranes. *Biophys. J. 89*, 1833–1840.

37. Fotiadis, D., Liang, Y., Filipek, S., Saperstein, D. A., Engel, A., and Palczewski, K. (2003) Atomic-force microscopy: Rhodopsin dimers in native disc membranes. *Nature 421*, 127–128.

38. Chabre, M., and le Maire, M. (2005) Monomeric G-protein-coupled receptor as a functional unit. *Biochemistry 44*, 9395–9403.

39. Mansoor, S. E., Palczewski, K., and Farrens, D. L. (2006) Rhodopsin self-associates in asolectin liposomes. *Proc. Natl. Acad. Sci. U.S.A. 103*, 3060–3065.

40. Botelho, A. V., Huber, T., Sakmar, T. P., and Brown, M. F. (2006) Curvature and hydrophobic forces drive oligomerization and modulate activity of rhodopsin in membranes. *Biophys. J. 91*, 4464–4477.

41. Maggio, R., Novi, F., Scarselli, M., and Corsini, G. U. (2005) The impact of G-protein-coupled receptor hetero-oligomerization on function and pharmacology. *FEBS J. 272*, 2939–2946.

42. Terrillon, S., and Bouvier, M. (2004) Roles of G-protein-coupled receptor dimerization. *EMBO Rep. 5*, 30–34.

43. Park, P. S., Filipek, S., Wells, J. W., and Palczewski, K. (2004) Oligomerization of G protein-coupled receptors: past, present, and future. *Biochemistry 43*, 15643–15656.

44. Milligan, G. (2004) G protein-coupled receptor dimerization: function and ligand pharmacology. *Mol. Pharmacol. 66*, 1–7.

45. Crocker, E., Eilers, M., Ahuja, S., Hornak, V., Hirshfeld, A., Sheves, M., and Smith, S. O. (2006) Location of Trp265 in metarhodopsin II: implications for the activation mechanism of the visual receptor rhodopsin. *J. Mol. Biol. 357*, 163–172.

46. Huber, T., Boetlho, A. V., Beyer, K., and Brown, M. F. (2004) Membrane model for the G-protein-coupled receptor rhodopsin: hydrophobic interface and dynamical structure. *Biophys. J. 86*, 2078–2100.